A Gap in the Highest Energy Cosmic Ray Spectrum as a Signature of Unification Scale Physics

Günter Sigl,* Sangjin Lee, David N. Schramm, Pijushpani Bhattacharjee

Recent experimental data seem to indicate that there is significant structure in the cosmic ray spectrum above 10^{18} electron volts (eV). Besides a dip at $\sim 5 \times 10^{18}$ eV, two events above 2×10^{20} eV have been observed. The implications for the existence of the Greisen-Zatsepin-Kuzmin cutoff, a long-lasting and still open question in cosmic ray physics, are discussed. This cutoff at a few times 10^{19} eV, caused by energy losses in the cosmic microwave background, has been predicted to occur in most acceleration models involving extragalactic sources. An acceleration origin of particles above 10^{20} eV within a few megaparsecs cannot be ruled out yet. However, persistence of the apparent gap in the existing data at a quadrupled total exposure would rule out many acceleration models at the 99 percent confidence level for any source distance. Particles above 10^{20} eV might then be directly produced by decay from some higher energy scale in contrast to acceleration of charged particles.

The cosmic microwave background has profound implications for the astrophysics of ultrahigh-energy cosmic rays (UHE CRs). Most notably, nucleons are subject to photopion losses on the cosmic microwave background, which leads to a steep drop in the interaction length at the threshold for this process at $\simeq 6 \times 10^{19}$ eV [the Greisen-Zatsepin-Kuzmin (GZK) effect] (*1*). For heavy nuclei, the giant dipole resonance that leads to photodisintegration produces a similar effect at $\simeq 10^{19}$ eV (*2*). One of the major unresolved questions in cosmic ray physics (*3*, *4*) is whether a cutoff exists in the UHE CR spectrum below 10^{20} eV that could be attributed to these effects if the sources are farther away than a few megaparsecs.

Recently, events with energies above the GZK cutoff have been detected (*5*–*10*). Most notably, the Fly's Eye experiment (*7*, *8*) and the Akeno array (*9*, *10*) each detected a superhigh-energy event significantly above 10^{20} eV with an apparent gap of about half a decade in energy between the highest and the second highest energy events. These findings led to a vigorous discussion on the nature and origin of these particles (*11*–*13*). In this report we show that the structure of the high-energy end of the UHE CR spectrum may provide powerful constraints on models for these extraordinary particles.

In "bottom-up" scenarios, charged baryonic particles are accelerated to the relevant UHEs, for example, by ordinary first-order Fermi acceleration at astrophysical shocks (*14*) or by linear acceleration in electric fields as they could arise in magnetic reconnection events (*15*). The resulting injection spectrum of the charged primaries at the source is typically a power law in energy E, $j_s(E) \propto E^{-q}$. In the case of reconnection acceleration there is no clear-cut prediction for the power law index q, but in the case of shock acceleration it satisfies $q \geq 2$. We refer to this latter case as conventional bottom-up acceleration scenarios. Secondary neutral particles like gamma rays and neutrinos are only produced by primary interactions in these scenarios (*16*).

In "top-down" scenarios, the primary particles, which can be charged or neutral, are produced at UHEs in the first place, typically by quantum mechanical decay of supermassive elementary X particles related to grand unified theories (GUTs). Sources of such particles at present could be topological defects left over from early universe phase transitions caused by the spontaneous breaking of symmetries underlying these GUTs (*17*). Generic features of top-down scenarios are injection spectra considerably harder (flatter) than in the case of bottom-up acceleration and a dominance of gamma rays in the X particle decay products (*18*). Even monoenergetic particle injection above the GZK cutoff can lead to rather hard spectra above the GZK cutoff (*19*).

The distinction between these scenarios is closely related to whether a GZK cutoff occurs in the form of a break in the spectrum. In contrast to the bottom-up scenario alone, the hard top-down spectrum can produce a pronounced recovery in the form of a flattening beyond the cutoff that could explain the highest energy events and possibly even a gap.

G. Sigl, S. Lee, D. N. Schramm, Department of Astronomy and Astrophysics, Enrico Fermi Institute, University of Chicago, Chicago, IL 60637–1433, USA, and National Aeronautics and Space Administration–Fermilab Astrophysics Center, Fermi National Accelerator Laboratory, Batavia, IL 60510–0500, USA.
P. Bhattacharjee, Indian Institute of Astrophysics, Sarjapur Road, Koramangala, Bangalore 560 034, India.
*To whom correspondence should be addressed.

For the statistical analysis, we assumed that the data are represented as the number of observed events, n_i, within a given energy bin i, where $i = 1, \ldots, N$. A given model predicts a certain observed differential flux $j(E)$ (in units of particles per unit area, unit time, unit solid angle, and unit energy). For any such model, the number of expected events, μ_i, in energy bin i is then given by

$$\mu_i = \int_{E_i^{\min}}^{E_i^{\max}} dE j(E) A(E) \qquad (1)$$

where $A(E)$ is the total experimental exposure at energy E (in units of area $\times$ solid angle $\times$ time), and bin i spans the energy interval $(E_i^{\min}, E_i^{\max})$. The Fly's Eye (*7*, *8*), Akeno (*9*, *10*), and Haverah Park (*5*) data are given in equidistant logarithmic energy bins of size $\log(E_i^{\max}/E_i^{\min}) = 0.1$ for the Fly's Eye and the Akeno data and 0.15 for the Haverah Park data. We combined these three data sets by adding the exposures, normalizing to the Fly's Eye bins, and using the suggested (*9*) systematic relative adjustment factors of 0.8 and 0.9 for the Akeno and Haverah Park energies, respectively. Because the bin sizes are smaller than the energy resolution, we interpolated linearly between the logarithmic Fly's Eye and Haverah Park bins.

The likelihood function L, adequate for the low statistics problem at hand, is then given by Poisson statistics as

$$L = \prod_{i=1}^{N} \frac{\mu_i^{n_i}}{n_i!} \exp(-\mu_i) \qquad (2)$$

Any free parameters of the theory are determined by maximizing the likelihood L in Eq. 2. In analogy to (*9*), we then determine the L significance for the given theory represented by the set of (optimal) μ_i's. The L significance is defined as the probability that this set of expectation values would by chance produce data with an L smaller than the L for the real data. This probability is calculated by drawing random data many times from Poisson distributions, whose expectation values are given by the set of μ_i's, and comparing the L of the random and the real data.

We performed the fits in the energy range between 10^{19} eV and the highest energy observed. For comparison, we computed separately the L significance of these fits in the range below the gap and in the range including the gap and the highest energy events. This demonstrates the influence of this structure on the fit quality.

In determining L, we also took the finite experimental energy resolution into account by folding the theoretical fluxes with a Gaussian window function in logarithmic energy space. The width of the Gaussian window function is determined by the en-

ergy resolution $\sigma_E^{(0)}$ for the present data, which is typically 30%. Future instruments such as the high-resolution Fly's Eye (*20*) that is under construction or the giant air shower detector proposed by the Pierre Auger project (*21*) will have an energy resolution of ≃10%.

Finally, for each model considered, we simulated data for an exposure increased by a factor f over the present exposure A_0, assuming the persistence of the apparent gap and the flux associated with the highest energy events in the existing data. For a given model this was done by determining the maximum L fit to the real data accounting for the energy resolution $\sigma_E^{(0)} \simeq 30\%$. This fixes the theoretical cosmic ray (CR) flux from which one can compute the corresponding set of expectation values $\mu_i(\sigma_E, A)$ $(i = 1, \ldots, N)$ for any energy resolution σ_E and exposure A. For all bins up to and including 10^{20} eV we then drew random event numbers n'_i from Poisson distributions with mean values given by $\mu_i(\sigma_E, A)$. For an unchanged energy resolution, $\sigma_E = \sigma_E^{(0)}$, we used $A = (f - 1)A_0$ and added the resulting random numbers n'_i to the numbers n_i of events already observed, whereas for simulating an enhanced energy resolution $\sigma_E = 10\%$ we used a fully random data set with $A = f A_0$. This procedure assumes that the underlying model represents the data well below the gap and continues to do so for increased exposure and a possible improved energy resolution. All other bins are assumed to contain the number of events n_i already observed, except for the two highest energy bins in which we place at least three more events in total. For the resulting data set, we computed the L significance of the underlying model as above. By doing this many times we determined for the given exposure enhancement the confidence level to which the given theory could be ruled out (or supported) if the gap structure should persist.

The five models we used for $j(E)$ (Table 1) are as follows. The Fly's Eye stereo data (*7*, *8*) show a significant dip in the spectrum at $\sim 5 \times 10^{18}$ eV. Bird and co-workers (*7*) attributed this dip to the superposition of a steeper galactic component, dominated by heavy nuclei, and a flatter extragalactic component of light particles such as nucleons or possibly also gamma rays. Above $\simeq 10^{19}$ eV, the extragalactic component would thus dominate, and a description by a power law is consistent with the existing data at least up to the GZK cutoff. Therefore, for model 1 we chose a power law with normalization and power law index q as free parameters. A power law continuing beyond the GZK cutoff could be produced in the following situations: First, there could be a nearby source (nearer than a few megaparsecs) of baryonic charged particles for which the (power law) injection spectrum is not noticeably modified and the GZK cutoff is irrelevant. Second, the observed flux could be dominated by neutral particles like gamma rays or even neutrinos (*13*) from a distant source (*22*). In contrast to nucleons, there are no resonance effects in the interactions of these particles around 10^{20} eV, so their processed spectrum would have a smooth shape that could be approximated by a power law. The fits typically result in $q \simeq 2.7$, and thus model 1 would belong to the bottom-up scenarios.

We also numerically calculated (*23*) the shape of the UHE CR spectrum from single sources at various distances and from uniformly distributed sources as it would be observed after propagation through the intergalactic medium. For all of these cases, we used power law injection of primary protons with cutoff energies $E_c \gg 10^{21}$ eV and normalizations determined by maximizing L. Our code accounts for the propagation of the nucleon component and secondary gamma-ray production as well as for gamma-ray propagation. Current experiments cannot distinguish between nucleons and a possible gamma-ray component, so we used the sum of their fluxes for $j(E)$. The secondary gamma-ray flux depends somewhat on the radio background and the extragalactic magnetic field B (*23*). To maximize the possible amount of recovery, we assumed a comparatively weak radio background with a lower cutoff at 2 MHz (*24*) and $B \ll 10^{-10}$ G. For injection indices $q \geq 2$, the resulting fluxes are representative of acceleration models of UHE CR origin. For the diffuse spectrum from a uniform source distribution, we assumed an absence of source evolution and chose $q = 2.3$ which fits the data quite well below the gap (see Table 2). The maximal source distance $d_{max} = 10^3$ Mpc was chosen in a range where d_{max} has no significant influence on the shape of

Table 1. Summary of models used for the fits to the data. The models consist of uniformly distributed sources (diffuse component), a single source (discrete component), or a combination of these. The source distance or range of source distances d and the power law injection index q are given. For a discrete source at $d = 0$, the power law injection spectrum is unmodified. The normalizations of the components are fitted to the data.

Model	Diffuse component		Discrete component	
	d (Mpc)	q	d (Mpc)	q
1	–	–	0	fitted
2	$0 \leq d \leq 10^3$	2.3	–	–
3	$0 \leq d \leq 10^3$	2.3	10	2.3
4	$30 \leq d \leq 10^3$	2.3	0	2.0
5	$30 \leq d \leq 10^3$	2.3	0	1.0

Table 2. L significances for fits of various models to the combined Fly's Eye monocular, Akeno, and Haverah Park data. The fits were performed between $10^{18.95}$ and $10^{20.55}$ eV. Significances are given for the energy range below and above $10^{20.05}$ eV separately.

Model	L significance	
	$10^{18.95}$ to $10^{20.05}$ eV	$10^{20.05}$ to $10^{20.55}$ eV
1	0.82	0.39
2	0.74	0.047
3	0.78	0.093
4	0.75	0.57
5	0.80	0.82

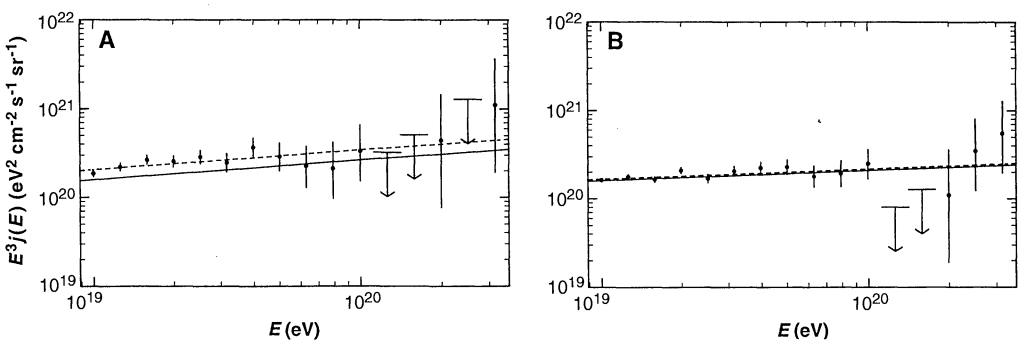

Fig. 1. Maximum L fits of the pure power law model 1 over the energy range $10^{18.95}$ eV $\leq E \leq 10^{20.55}$ eV. We fitted the effective flux (dashed lines) that results from the real differential flux (solid lines) by taking the experimental energy resolution into account. The data are given as 68% C.L. error bars or as 84% C.L. upper limits. For illustration purposes we multiplied the steeply falling flux by E^3. (**A**) Fit to the combined Fly's Eye monocular, Akeno, and Haverah Park data with ≃30% energy resolution, corresponding to an L significance of 39% above 10^{20} eV. (**B**) A typical example resulting from "data" simulated for a quadrupled exposure with 10% energy resolution. For these data, model 1 would be ruled out at the 99% C.L.

the resulting spectrum above 10^{19} eV. The minimal source distance d_{min} was roughly chosen by maximizing the fit quality.

A discrete source beyond a few megaparsecs alone cannot explain the data including the highest energy events. More interesting cases are a diffuse spectrum alone (model 2) and its combination with an additional discrete source at 10 Mpc (model 3), where in both cases $d_{min} = 0$. In model 4 we combined a diffuse spectrum for $d_{min} =$ 30 Mpc with a nearby source, represented by an unprocessed power law with index $q = 2$. This model could be relevant if there were a strong galactic source that accelerates iron nuclei much beyond 10^{20} eV with the hardest injection spectrum possible for shock acceleration models ($q = 2$).

In top-down models, the flux above the GZK cutoff could be dominated by gamma rays (*18*), so the processed spectrum is somewhat uncertain because of interactions with unknown backgrounds (*23*). However, the hard top-down component must be negligible below the GZK cutoff, whereas above the cutoff it can be approximated by a power law. In a manner similar to model 4, we chose best fit combinations of the diffuse bottom-up spectrum for $d_{min} = 30$ Mpc with an unprocessed power law of index $q = 1$ as our model 5. Because of gamma-ray propagation effects (*23*), the injection spectrum corresponding to this latter hard component could be considerably softer and consistent with various constraints on energy injection as long as the X particle mass is not too high (*25*). Model 5 acts as a generic example of how an additional hard top-down component might naturally produce a pronounced recovery (spectral flattening). In fact, for $q < 1$ the number of events expected per logarithmic energy bin even starts to grow with energy beyond a few times 10^{20} eV, although the actual differential flux is always a decreasing function of energy. Indeed, this can naturally give rise to a gap in the measured spectrum.

Table 3. Same as for Table 2 but with "simulated data" for a quadrupling of experimental exposures, assuming persistence of the gap structure. *L* significances are listed only for the energy range above 10^{20} eV. The results are given for both the energy resolution of present instruments, $\sigma_E^{(0)} \simeq$ 30%, and an improved energy resolution, $\sigma_E \simeq$ 10%, expected for future instruments. A high-energy resolution is advantageous mainly for determining the significance of models of the type 4 and 5, which predict a break followed by a recovery.

Model	*L* significance for $10^{20.05}$ to $10^{20.55}$ eV at σ_E of	
	30%	10%
1	≲0.002	≲0.01
2	≲0.006	≲0.003
3	≲0.01	≲0.01
4	≲0.10	≲0.15
5	≃0.35	≃0.55

The results for the combined Fly's Eye monocular, Akeno, and Haverah Park data for the models discussed above are presented in Table 2. Below the gap, the one-component models 1 and 2 both yield reasonably good fits. Additional discrete sources beyond a few megaparsecs (model 3) do not improve the fit significantly over a pure diffuse spectrum (model 2). Thus, there is no indication of a significant "bump" below the GZK cutoff that would be produced by strong discrete sources (*26*). If one includes the gap and the highest energy events into consideration, an exclusive diffuse bottom-up component is ruled out at the 95% confidence level (C.L.). In contrast, bottom-up sources nearer than a few megaparsecs are still consistent with the data at the 1σ level. Nevertheless, because there are no obvious visible source candidates near the arrival directions of the highest energy events observed, this is a highly problematic option, as was argued in (*12*). We fit the power law model 1 to the combined data from 10^{19} eV up to the highest energy event (Fig. 1A). The best fits in this energy range, however, are produced by combinations of a diffuse component with a hard unprocessed power law (models 4 and 5). The result for the exotic model 5 is shown in Fig. 2A.

We simulated "data" for a quadrupled exposure, assuming persistence of the gap and a substantial flux above 2×10^{20} eV (Table 3). The constraints on the models become much more stringent. A typical example for fitting model 1 to data simulated for a quadrupled exposure is shown in Fig. 1B. Indeed, all curves predicted from bottom-up models (model 1 to 4) can be ruled out at least at the 99% C.L., except for the most optimistic bottom-up model, model 4, involving a strong nearby (supposedly iron) source, which in the case of 10% energy resolution could be ruled out only at the ~85% C.L. The basic reason is that local sources can reproduce the superhigh-energy events but at the same time predict events in the gap which are not seen. Sources beyond about 20 Mpc, on the other hand, predict a GZK cutoff and a recovery that is much too weak to explain the highest energy events. This conclusion can only be evaded if either the systematic energy uncertainties are much larger than the estimated energy resolution or the acceleration spectra are hardened by unexpected propagation effects. This could happen, for example, by energy-dependent diffusion in a galactic magnetic field extending far into the galactic halo.

In contrast, the representative model with a top-down component is typically consistent at the 1σ level. A typical situation where the model 5 is fitted to simulated data is shown in Fig. 2B. Thus, if the observed gap structure should persist within a quadrupling of the data set and the above mentioned caveats can be excluded in the future, it would be a statistically significant proof of the need for new physics. This need would become even more pressing if high fluxes would continue considerably beyond the highest energies detected to date. Conversely, if the gap structure should disappear and the flux in the highest energy bins is not too high, there would be no immediate need for new physics except for the nontrivial problem of acceleration to such high energies (*27*). A decisive answer should be possible within the Pierre Auger project (*21*) which would allow an exposure enhancement by much more than a factor of 4. This project should also allow the com-

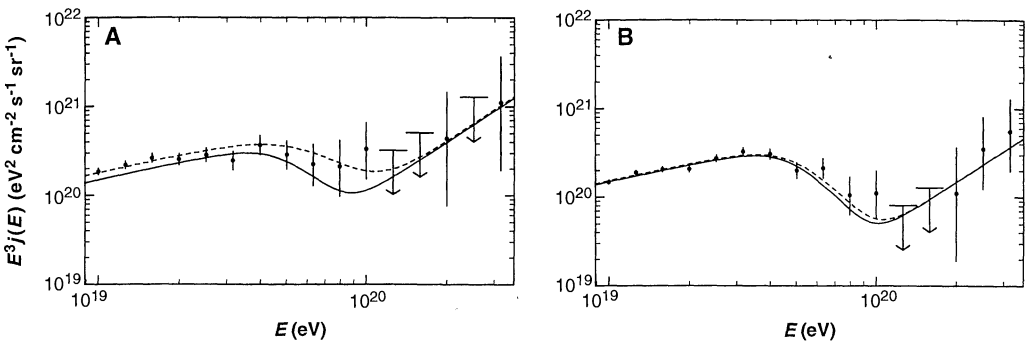

Fig. 2. Same as Fig. 1 but for the exotic model 5. In contrast to the pure power law model 1, the *L* significance above 10^{20} eV [82 and 60% in the case of (**A**) and (**B**), respectively] typically stays within the 1σ level for both exposures.

position and anisotropy of the UHE CR flux to be measured, which would provide additional information on its origin.

REFERENCES AND NOTES

1. K. Greisen, *Phys. Rev. Lett.* **16**, 748 (1966); G. T. Zatsepin and V. A. Kuzmin, *Pis'ma Zh. Eksp. Teor. Fiz.* **4**, 114 (1966) [*J. Exp. Theor. Phys.* **4**, 78 (1966)]; F. W. Stecker, *Phys. Rev. Lett.* **21**, 1016 (1968).
2. J. L. Puget, F. W. Stecker, J. H. Bredekamp, *Astrophys. J.* **205**, 638 (1976).
3. M. Nagano and F. Takahara, Eds., *Astrophysical Aspects of the Most Energetic Cosmic Rays* (World Scientific, Singapore, 1991).
4. Proceedings of the *Tokyo Workshop on Techniques for the Study of Extremely High Energy Cosmic Rays*, Tokyo, 27 to 30 September 1993 (Institute for Cosmic Ray Research, Univ. of Tokyo, 1993).
5. M. A. Lawrence, R. J. O. Reid, A. A. Watson, *J. Phys. G Nucl. Part. Phys.* **17**, 733 (1991); A. A. Watson, in (*3*), p. 2.
6. N. N. Efimov *et al.*, in (*3*), p. 20; T. A. Egorov, in (*4*), p. 35.
7. D. J. Bird *et al.*, *Phys. Rev. Lett.* **71**, 3401 (1993); *Astrophys. J.* **424**, 491 (1994).
8. D. J. Bird *et al.*, *Astrophys. J.* **441**, 144 (1995).
9. S. Yoshida *et al.*, *Astropart. Phys.* **3**, 105 (1995).
10. N. Hayashida *et al.*, *Phys. Rev. Lett.* **73**, 3491 (1994).
11. J. P. Rachen, T. Stanev, P. L. Biermann, *Astron. Astrophys.* **273**, 377 (1993); J. W. Elbert and P. Sommers, *Astrophys. J.* **441**, 151 (1995).
12. G. Sigl, D. N. Schramm, P. Bhattacharjee, *Astropart. Phys.* **2**, 401 (1994).
13. F. Halzen, R. A. Vazquez, T. Stanev, H. P. Vankov, *ibid.* **3**, 151 (1995).
14. A. M. Hillas, *Annu. Rev. Astron. Astrophys.* **22**, 425 (1984).
15. C. A. Haswell, T. Tajima, J.-I. Sakai, *Astrophys. J.* **401**, 495 (1992).
16. S. Yoshida and M. Teshima, *Prog. Theor. Phys.* **89**, 833 (1993).
17. P. Bhattacharjee, C. T. Hill, D. N. Schramm, *Phys. Rev. Lett.* **69**, 567 (1992).
18. F. A. Aharonian, P. Bhattacharjee, D. N. Schramm, *Phys. Rev. D* **46**, 4188 (1992).
19. J. Geddes, T. C. Quinn, R. M. Wald, *Astrophys. J.*, in press.
20. D. J. Bird *et al.*, Proceedings of the *Twenty-Fourth International Cosmic Ray Conference*, Rome, 28 August to 8 September 1995 (Instituto Nazionale Fisca Nucleare, Rome, 1995), vol. 2, pp. 504–507.
21. Proceedings of the International Workshop on Techniques to Study Cosmic Rays with Energies $\geq 10^{19}$ eV, Paris, 22 to 24 April 1992, M. Boratav *et al.*, Eds., *Nucl. Phys. B* **28B** (1992), (Proc. suppl.).
22. G. Sigl and S. Lee, in (*20*), pp. 356–359.
23. S. Lee and G. Sigl, in preparation.
24. T. A. Clark, L. W. Brown, J. K. Alexander, *Nature* **228**, 847 (1970).
25. X. Chi, C. Dahanayake, J. Wdowczyk, A. W. Wolfendale, *Astropart. Phys.* **1**, 239 (1993); G. Sigl, K. Jedamzik, D. N. Schramm, V. S. Berezinsky, Fermilab publication 95/051-A, *Phys. Rev. D.*, in press; R. J. Protheroe and P. A. Johnson, *Astroparticle Phys.*, in press.
26. C. T. Hill and D. N. Schramm, *Phys. Rev. D* **31**, 564 (1985).
27. For a recent account see, for example, C. A. Norman, D. B. Melrose, A. Achterberg, *Astrophys. J.* **454**, 60 (1995).

28. We gratefully acknowledge J. W. Cronin, S. Yoshida, and P. Sommers for reading the manuscript and giving valuable suggestions. Supported by the Department of Energy (DOE), NSF, and the National Aeronautics and Space Administration (NASA) at the University of Chicago, by the DOE and by NASA through grant NAG5-2788 at Fermilab, and by the Alexander-von-Humboldt Foundation. S.L. acknowledges the support of the POSCO Scholarship Foundation in Korea. P.B. wishes to thank R. Kolb and J. Frieman for hospitality and support at Fermilab at the beginning stages of this work.

12 June 1995; accepted 14 September 1995

Selective Trafficking of KNOTTED1 Homeodomain Protein and Its mRNA Through Plasmodesmata

William J. Lucas,* Sabine Bouché-Pillon, David P. Jackson, Lynda Nguyen, Lucian Baker, Biao Ding,† Sarah Hake

Plasmodesmata are intercellular organelles in plants that establish cytoplasmic continuity between neighboring cells. Microinjection studies showed that plasmodesmata facilitate the cell-to-cell transport of a plant-encoded transcription factor, KNOTTED1 (KN1). KN1 can also mediate the selective plasmodesmal trafficking of *kn1* sense RNA. The emerging picture of plant development suggests that cell fate is determined at least in part by supracellular controls responding to cellular position as well as lineage. One of the mechanisms that enables the necessary intercellular communication appears to involve transfer of informational molecules (proteins and RNA) through plasmodesmata.

Cell fate in higher plants is determined by position rather than by lineage (*1*). Although environmental and hormonal signals could act in a cell-autonomous manner to control cell fate, clonal analysis of developmental mutants has indicated that cell-to-cell transport, as part of a longer chain of signaling events, may be involved in the orchestration of developmental events (*2*). For example, expression of the gene *Floricaula* (to produce FLO), which affects meristem identity in *Antirrhinum majus* (snapdragon) in only the outer (epidermal) layer (L1) of the meristem, activates downstream genes involved in flower development (*3*) in adjacent cell layers. Similarly, the genotype of the inner layer (L3) of the tomato floral meristem controls development of the outer layers (L2 and L1) (*4*). These findings are consistent with the hypothesis that FLO and the fasciated gene product of tomato potentiate cellular interactions among the three layers of the floral meristem.

Although such intercellular control may be mediated by cell surface receptors and soluble ligands, it may also involve the selective cell-to-cell transport of proteins through plasmodesmata, the specialized, plasma membrane–lined cytoplasmic pores that maintain cytoplasmic and endomembrane continuity between many cells in the plant (*5*). These pores are the route by which viral movement proteins, which are essential for the spread of infection in plants (*6*), mediate trafficking of viral RNA and DNA (*6*–*8*). The viral movement proteins seem to interact with an endogenous plasmodesmal macromolecular trafficking pathway.

Here we report an analysis of movement of the protein and RNA encoded by the maize *knotted1* (*kn1*) homeobox gene (*9*). Ectopic expression of *kn1* in the vascular tissue of

W. J. Lucas, S. Bouché-Pillon, L. Nguyen, L. Baker, B. Ding, Section of Plant Biology, Division of Biological Sciences, University of California, Davis, CA 95616, USA. D. P. Jackson and S. Hake, U.S. Department of Agriculture–University of California Berkeley Plant Gene Expression Center, Albany, CA 94710, USA.

*To whom correspondence should be addressed.
†Present address: Department of Botany, Oklahoma State University, Stillwater, OK 74078, USA.

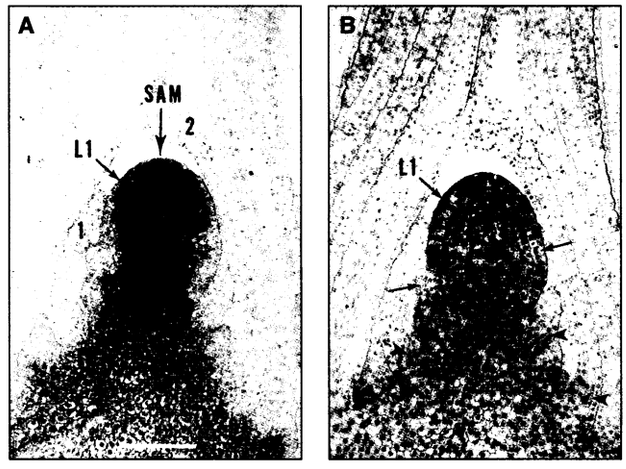

Fig. 1. Serial sections of a maize vegetative shoot apex processed for in situ hybridization for *kn1* mRNA (**A**) and immunolocalization of KN1 (**B**) reveal the presence of KN1 in L1 cells in which its mRNA is not detected. The shoot apical meristem (SAM) is flanked by leaf primordia [1 and 2 in (A)] and older expanding leaves in which *kn1* mRNA and KN1 are not detected. Regions in the SAM that lack KN1 [unlabeled arrows in (B)] predict the position of leaf primordial development. L1, outer cell layer of the SAM. Note that KN1 is present in a few cells across the base of each developing leaf (arrowheads). Scale bar, 100 μm.